New Journal of Physics
The open access journal at the forefront of physics

Deutsche Physikalische Gesellschaft DPG IOP Institute of Physics

PAPER • OPEN ACCESS

Modeling of electron emission processes accompanying radon-α-decays within electrostatic spectrometers

To cite this article: N Wandkowsky *et al* 2013 *New J. Phys.* **15** 083040

New Journal of Physics
The open access journal for physics

Modeling of electron emission processes accompanying radon-α-decays within electrostatic spectrometers

N Wandkowsky[1,5], G Drexlin[1], F M Fränkle[1,2], F Glück[1,3], S Groh[1] and S Mertens[1,4]

[1] KCETA, Karlsruhe Institute of Technology, D-76131 Karlsruhe, Germany
[2] Department of Physics, University of North Carolina, Chapel Hill, NC, USA
[3] Research Institute for Nuclear and Particle Physics, Theory Department, Budapest, Hungary
[4] Institute for Nuclear and Particle Astrophysics, Lawrence Berkeley National Laboratory, CA, USA
E-mail: nancy.wandkowsky@kit.edu

New Journal of Physics **15** (2013) 083040 (16pp)
Received 4 April 2013
Published 21 August 2013
Online at http://www.njp.org/
doi:10.1088/1367-2630/15/8/083040

Abstract. Electrostatic spectrometers utilized in high-resolution β-spectroscopy studies such as in the Karlsruhe Tritium Neutrino (KATRIN) experiment have to operate with a background level of less than 10^{-2} counts per second. This limit can be exceeded by even a small number of ^{219,220}Rn atoms being emanated into the volume and undergoing α-decay there. In this paper we present a detailed model of the underlying background-generating processes via electron emission by internal conversion, shake-off and relaxation processes in the atomic shells of the ^{215,216}Po daughters. The model yields electron energy spectra up to 400 keV and electron multiplicities of up to 20 which are compared to experimental data.

[5] Author to whom any correspondence should be addressed.

Contents

1. Introduction

The Karlsruhe Tritium Neutrino experiment (KATRIN) is a next generation, large-scale tritium β-decay experiment designed to determine the effective electron (anti-) neutrino mass $m_{\bar{\nu}_e}$ with a sensitivity of 200 meV (90% confidence level (CL)) [1]. It is currently being assembled by an international collaboration at the Karlsruhe Institute of Technology (KIT) in Germany.

KATRIN will investigate the kinematics of tritium β-decay with unprecedented precision in a narrow region close to the β-decay endpoint $E_0 \approx 18.6$ keV [2]. It is only in this narrow region with almost vanishing neutrino momenta that one can gain access to $m_{\bar{\nu}_e}$. An essential pre-requisite to obtain the reference sensitivity of 200 meV is a low background level of $<10^{-2}$ counts per second (cps) in the signal region close to E_0.

The KATRIN setup is described in detail in [1]. It consists of a windowless gaseous tritium source providing $>10^{11}$ β-decays per second, a differential and cryogenic pumping section to eliminate the injected tritium molecules from the beam line, as well as an electrostatic spectrometer acting as high-pass energy filter of unprecedented precision, and finally a position sensitive detector to count transmitted electrons. This work is focused on background processes in the large spectrometer section.

In a previous publication [3] we have reported on measurements with the KATRIN pre-spectrometer in a test setup configuration where α-decays of ^{219,220}Rn atoms in the volume of an electrostatic spectrometer of the MAC-E filter type[6] [4–6] were identified as significant source of background. These atoms originate mainly from the non-evaporable getter (NEG) material which is used as a chemical pump to obtain ultra-high vacuum (UHV) conditions of $p \leqslant 10^{-10}$ mbar [7], but also from other auxiliary equipment within the spectrometer vessel and from the stainless steel vessel hull itself. In particular, we could demonstrate that a single radon α-decay can produce up to several thousands of detector hits in the energy region-of-interest over an extended time period of up to several hours. This background originates from the emission of electrons in the energy range from eV up to several hundreds of keV, which

[6] Magnetic adiabatic collimation with electrostatic filter.

is caused by a variety of processes related to the emission of the energetic α-particle as well as the subsequent reorganization of the atomic shells. Almost all of these electrons are trapped in the sensitive volume of the spectrometer due to the known magnetic bottle characteristic of a MAC-E filter [8, 9]. Owing to the excellent UHV conditions in this part of the setup, electrons remain trapped over very long time periods, so that they can produce secondary electrons via ionization of residual gas molecules. A significant fraction of these secondaries can reach the detector, resulting in a background rate exceeding the KATRIN design limit of 10^{-2} cps.

In this paper we describe a detailed model of electron emission processes following α-decays of the isotopes ^{219,220}Rn. In a separate publication [10] we validate in detail this model experimentally by making use of precise electron trajectory calculations in a MAC-E filter to describe the initial background investigations reported in [3, 11, 12], as well as the more in-depth studies performed in [10, 13]. Furthermore, we make use of the model of this work to derive estimates of the background rates and topologies for the final KATRIN setup in [9], while an active background reduction technique concerning trapped electrons is described in [14].

This paper is organized as follows. Section 2 will present in detail the processes related to electron emission during and after ^{219,220}Rn α-decay, namely internal conversion (IC), inner-shell shake-off (SO), relaxation (RX) and atomic shell reorganization (SR). The implementation of this model into our simulation software will be discussed in section 3. Within section 4 we will outline the importance of the physics model implemented in this work in the light of our attendant publications [9, 10, 14].

2. Electron emission accompanying radon α-decay

An essential design feature of high-resolution tritium β-spectroscopy by a MAC-E filter is an excellent UHV in the pressure range $p \leqslant 10^{-10}$ mbar, so that background-generating ionization processes of β-decay electrons during the filter process are minimized. In the case of the KATRIN spectrometers, this is achieved by NEG strips totaling a length of 3 km in the main spectrometer and 90 m in the pre-spectrometer. As shown in [3], the large surface of the porous NEG strips gives rise to emanation of radon atoms associated with the primordial ^{232}Th, ^{235}U and ^{238}U decay chains (see figure 1). Furthermore, the large stainless steel surface of the spectrometer vessel (main spectrometer: 650 m^2, pre-spectrometer: 25 m^2) and auxiliary equipment attached to it also contributes to radon emanation due to small quantities of radon progenitors contained near the surface.

The pump out time of radon in the KATRIN spectrometers is $t_{\mathrm{prespec}} \approx 25$ s for the pre-spectrometer and $t_{\mathrm{mainspec}} \approx 360$ s for the larger main spectrometer. Due to the comparably long half-life of $t_{1/2}(^{222}\mathrm{Rn}) = 3.82$ d [15], the isotope ^{222}Rn is essentially being pumped out of the spectrometer before it decays. Therefore, its background contribution can be neglected. The short-lived isotopes ^{219}Rn ($t_{1/2} = 3.96$ s) and ^{220}Rn ($t_{1/2} = 55.6$ s), however, will α-decay uniformly over the entire spectrometer volume ($V_{\mathrm{prespec}} = 8.5\,\mathrm{m}^3$, $V_{\mathrm{mainspec}} = 1250\,\mathrm{m}^3$) to their respective daughter nuclei ^{215}Po and ^{216}Po (see figure 1). The important fact for our investigations here is that all α-decays are accompanied by the emission of atomic shell electrons from the eV up to the multi-keV scale (the α-particle as well as x-ray fluorescence photons are of no interest for our background studies, see [9]). If these electrons are emitted into the sensitive volume of the spectrometer, they can contribute significantly to the background rate via secondary processes.

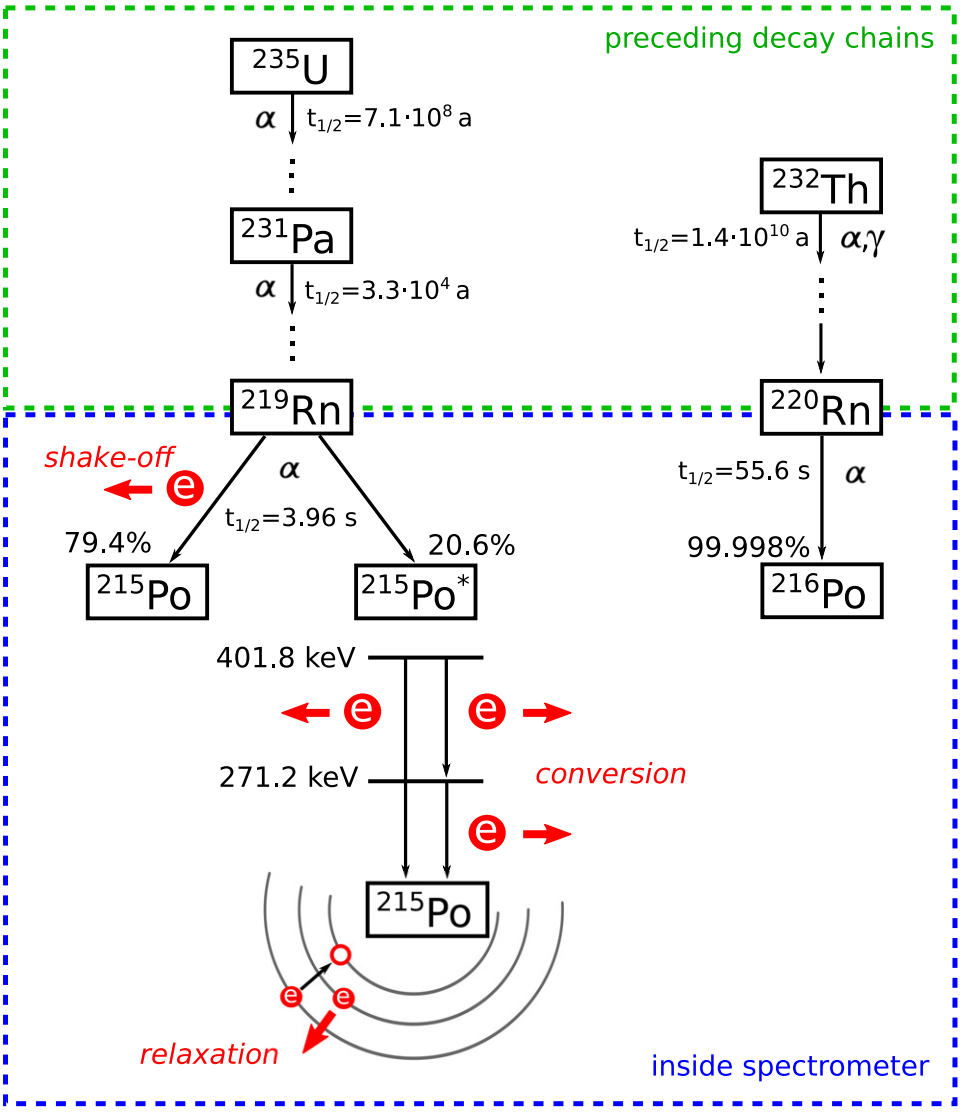

Figure 1. Top: in the KATRIN spectrometers, non-equilibrium decay chains lead to emanation of the two short-lived radon isotopes ^{219}Rn and ^{220}Rn. Bottom: radon α-decay processes inside the spectrometer and subsequent electron emission processes resulting from SO (both isotopes), conversion (mainly ^{219}Rn) and shell RX (following conversion and SO processes).

There are various processes which can result in the emission of more than a dozen electrons in a single α-decay. If the α-decay populates an excited level of the daughter nucleus, the process of IC, as described in section 2.1, will result in the emission of electrons with energies of up to several hundreds of keV. Also, the α-particle itself can interact with electrons of the inner atomic shells, leading to so called SO processes, detailed in section 2.2. Both processes produce vacancies in the electron shells. These are successively filled by atomic RX processes, which are the focus of section 2.3. Finally, the SR process of outer shell electrons is described in section 2.4.

Table 1. The table gives an overview of the relative probabilities P_i (per α-decay) of the dominant IC lines and of the corresponding electron energies E_{kin} for ^{219}Rn, as measured by Browne [18]. The electron energy is given by (1) and can thus be attributed to specific excited levels of energy E^* via the known values of the binding energy E_b (K: 93.1 keV; L: 16.9 keV; M: 4.1 keV; and N: 1 keV). Only electron lines with an emission probability larger than 0.05% are given. In our model we incorporate the possibility of consecutive IC processes within a single α-decay in case that the 401.81 keV level of ^{215}Po* is populated and de-excites to the 271.23 keV level.

E_{kin} (keV)	P_i (%)	Shell	E^* (keV)
37.50	0.40	K	130.60
113.66	0.13	L	130.60
178.13	1.27	K	271.23
254.29	0.74	L	271.23
267.08	0.19	M	271.23
270.24	0.06	NP	271.23
308.71	0.23	K	401.81
384.87	0.10	L	401.81

2.1. Internal conversion

In an IC process the excited level of the daughter nucleus, which is populated by the α-decay process, interacts electromagnetically with an inner-shell electron, which thus is emitted from the atom. As the IC process is competing with radiative processes, it is only dominant for heavy nuclei ($P(\mathrm{IC}) \propto Z^3$) [16, 17], as is the case for polonium ($Z = 84$). In addition, the probability of IC decreases for larger transition energies, so it is relevant only for low-lying levels. In our specific case, IC processes are thus of importance only for $^{219}\mathrm{Rn} \rightarrow ^{215}\mathrm{Po}^*$ decays, where significant branching ratios lead to the two excited levels ($7/2^+$, 271.2 keV and $5/2^+$, 401.8 keV) shown in figure 1. In case of $^{220}\mathrm{Rn} \rightarrow ^{216}\mathrm{Po}$ decays, the even-even nucleon configuration of the ^{216}Po daughter creates a paucity of low-lying excited states, implying that IC processes following α-decays of ^{220}Rn are exceedingly rare processes.

In an IC process, an inner-shell electron with binding energy E_b is emitted into the continuum with a kinetic energy of

$$E_{kin} = E^* - E_b, \tag{1}$$

where E^* denotes the excitation energy of the nucleus. For our specific case of ^{215,216}Po* daughters, conversion electron energies between about 40 and 500 keV are observed [18, 19].

The total conversion probability amounts to about 3.3% when integrating over all electron shells in the case of ^{215}Po*. The probability is largest for K-shell electrons (2%) as they are closest to the nucleus. Table 1 lists the dominant electron emission probabilities and electron energies for the decay $^{219}\mathrm{Rn} \rightarrow ^{215}\mathrm{Po}^*$ [18]. Our model allows for consecutive IC processes in case the initial de-excitation process does not result in a ground state configuration of the polonium daughter. We also include the rare IC process of the decay $^{220}\mathrm{Rn} \rightarrow ^{216}\mathrm{Po}^*$ [19], but its contribution is negligible for the investigations in [9, 10]. As mentioned above, the emission

Table 2. SO probabilities for electrons from specific inner shells in ^{210}Po, as measured by Rapaport *et al* [24, 25].

Shell	Probability (%)
K [24]	1.6×10^{-4}
LI [25]	5.1×10^{-2}
LII [25]	0.6×10^{-2}
LIII [25]	1.5×10^{-2}
M [25]	1.8

of a conversion electron leaves a vacancy in the electron shell, leading to subsequent complex atomic shell RX processes, which are described in sections 2.3 and 2.4.

2.2. Inner shell shake-off processes

A nuclear α-decay leads to a perturbation of the atomic shells, as the electrons experience the passage of the outgoing α-particle through the atomic orbitals, as well as the sudden change $\Delta Z = Z' - Z$ of the Coulomb potential of the nucleus (initial state: $Z = 86$ for radon, final state: $Z' = 84$ for polonium) [20]. The impact of both processes on inner-shell (K, L, M) electrons is different than on outer shell (N or higher) electrons due to the largely different orbital velocities. For inner-shell electrons, the orbital period is much larger than the orbital passage time of the α-particle ($v_\alpha / v_e \approx 0.1$, with v_e the electron orbital velocity and v_α the α-particle velocity). For outer shell electrons, this ratio is reversed ($v_e / v_\alpha \approx 0.1$). Accordingly, inner-shell electrons will adjust adiabatically to the sudden change of nuclear charge. Outer shell electrons, however, remain 'frozen' in their parent atom ground state ($6p^6$ for radon) and will only slowly rearrange to the daughter orbitals ($6p^4$ for polonium), see section 2.4.

For inner shells, electron SO is caused by the direct collision process [20–22]. In this case, the α-particle, which has already gained 99% of its final kinetic energy inside the mean radius of the K-shell, can exchange energy with an electron via the Coulomb interaction when passing in the vicinity of the corresponding orbital, and, consequently, it can kick out the inner-shell electron into the continuum. The decay energy is shared between the α-particle and the emitted electron. The latter carries only a small fraction, usually of the same order of magnitude as the shell binding energy E_b. Therefore, in the adiabatic transition, the SO process results in a continuous, steeply falling energy spectrum. In this work we use the parameterization of Bang and Hansteen [23] to determine the emission probability for a SO electron with a certain kinetic energy E_{shake}:

$$N(E_{shake}) = \left(\frac{E_b}{E_b + E_{shake}} \right)^8 . \tag{2}$$

The SO probabilities for ^{210}Po have been measured [24–26] and calculated [21, 27] and are used as a good approximation for the ^{215,216}Po isotopes which are considered here. The values, which are listed in table 2, underline the well-known fact that the ejection probability strongly increases for higher shells. For the M-shell, only the total emission probability is listed. In our model, we do, however, consider the five subshells individually, adapting the corresponding emission probabilities. Since there was no experimental data available for the individual subshells, we used an equal distribution amongst the subshells as an approximation.

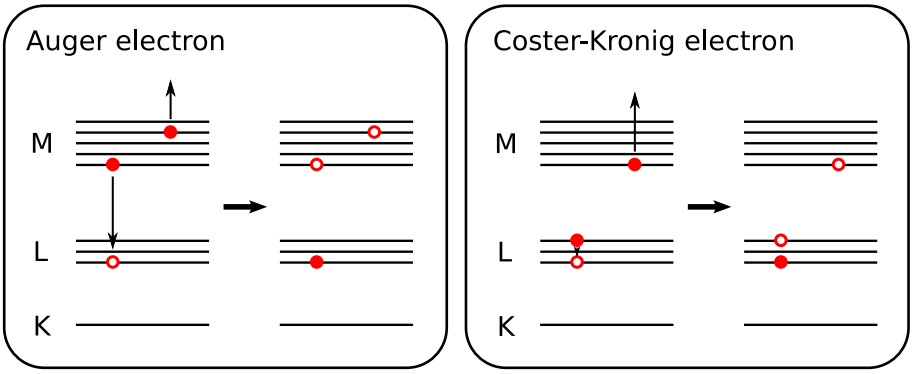

Figure 2. Sketch of a RX process. An inner-shell vacancy is filled by an electron from an outer shell or a neighboring subshell, thereby releasing the corresponding binding energy difference. This energy can be transferred to another electron, which is then ejected from the atom. Depending on the origin of the electron filling the vacancy, the emitted electrons are called Auger electrons or Coster–Kronig electrons.

2.3. Relaxation following conversion and shake-off processes

An electron, which is emitted via an IC or SO process, will leave a vacancy in an inner shell, as shown schematically in figure 2. As a consequence, the electron structure of the atom has to rearrange, thereby releasing binding energy. This can be either in the form of a fluorescence photon (radiative transition), which is of no concern for this work, or in the form of an Auger electron, if the electron filling the vacancy originates from a different shell, or a Coster–Kronig electron, in case it is emitted from a subshell of the same level (non-radiative transition) [28]. In case of a radiative transition, the initial vacancy is transferred to a higher atomic shell, while for non-radiative transitions the atomic shells are left with two vacancies. The RX processes then propagate up to the outermost shell. In heavy atoms such as polonium, large cascades are observed when inner-shell vacancies are successively filled by non-radiative transitions ('Auger explosions'). Consequently, highly charged polonium ions are created, which cannot be neutralized when propagating in the spectrometer UHV environment[7].

An electron emitted in a non-radiative transition will receive a distinct kinetic energy. In the example of figure 2, the Auger electron energy can, in a first approximation, be determined by

$$E_{\mathrm{kin}} = (E_{\mathrm{b,L1}} - E_{\mathrm{b,M1}}) - E_{\mathrm{b,M4}}, \tag{3}$$

where $E_{\mathrm{b},i}$ are the binding energies of the involved shells i. In case of a radiative transition, the photon would have received the energy difference $E_\gamma = E_{\mathrm{b,L1}} - E_{\mathrm{b,M1}}$. The above approximation neglects two effects [29]:

- A pair of holes in the atomic orbitals retains interaction energy.
- The RX of the atomic orbitals results in a lowering of the final state energy, which alters the ionization energies of electron shells containing holes.

[7] The highly charged Po-ion will be neutralized when hitting the spectrometer vessel.

The Auger electron energies, which are applied in our model, are indeed corrected for the aforementioned effects, using the intermediate coupling model of [29]. In the case of polonium, RX electron energies can reach up to about 93 keV, which approximately corresponds to the K-shell binding energy.

Sudden changes of the atomic potentials occur during vacancy cascade development, which can lead to the emission of electrons [30]. However, due to their relatively low emission probabilities, this effect is only of minor importance and is neglected in our model.

Furthermore, as the number of vacancies in the atomic shells increases, the electron binding energies decrease which can lead to the closure of some Coster–Kronig channels, reducing the average charge state of the daughter atom [30]. Neglecting this effect does not significantly influence the simulation results for two reasons:

- The thereby omitted electrons are predominantly of exceedingly low energies <100 eV. Due to their low magnetic storage probability (electrons with transversal kinetic energies of less than 60 eV are not stored), these are not able to produce a significant amount of secondary electrons and hence contribute only marginally to the background.
- Additionally, they accompany at least one high-energy IC and inner-shell SO electron, which generates several hundred or even thousand secondary electrons due to the magnetic storage in the spectrometer.

2.4. Atomic shell reorganization

In the processes described above the atomic shell of the polonium daughter is left in an excited state, and the de-excitation follows a rather complex scheme involving many different pathways within RX cascades. If the α-decay process leaves the atomic shell unperturbed, or if the SO process of the α-particle involves outer shell (N or higher) electrons, the RX processes are much less complex. The underlying effect is that the outer shell electron wave function cannot adjust adiabatically to the final state due to the fact that the outer shell electron velocity is much smaller than the α-particle velocity. In any case the atomic system will relax to the smaller $(Z-2)$ nuclear charge of the daughter nucleus.

There is a gradual transition between α-decay processes, which result in a highly excited final state, and those resulting in a configuration where the atomic shell is virtually unperturbed. In the latter case, the initial state with the shell configuration of radon ($6p^6$) has to adjust to the ground state shell configuration of polonium ($6p^4$). In our model we treat the involved SR processes in an identical manner.

The change in nuclear charge $(Z-2)$ in the α-decay ${}_{86}\mathrm{Rn} \rightarrow {}_{84}\mathrm{Po}$ results in a change $\Delta E = 37.7$ keV in the total binding energy of the atomic electrons if the relativistic Hartree–Fock–Slater calculations of Lu [31] are used. ΔE is composed of the sudden energy exchange component ΔE_{sud} and the much slower rearrangement component ΔE_{R} [22]. As the fast inner electrons can adjust adiabatically to the effective nuclear charge reduction by rearranging to daughter orbitals, almost all of ΔE occurs suddenly (ΔE_{sud}) and has to be supplied by the outgoing α-particle, which results in an equivalent retardation. The remaining small fraction ΔE_{R} is retained by the atom as temporary excitation energy for the much slower shell rearrangement in the outer shells. We employ a scenario where the average atomic rearrangement energy $\overline{\Delta E_{\mathrm{R}}}$ ($6p^6 \rightarrow 6p^4$) of about 250 eV [22] is shared statistically by two electrons from the outermost shells. If their kinetic energy is larger than the polonium ionization

energy for P-shell electrons (1–9 eV), they are emitted into the continuum. This results in a flat energy spectrum of low-energy 'SR' electrons.

As the probability for inner-shell SO (see table 2) and IC (see table 1) is not dominating, the above described atomic SR in the ground state configuration is the most frequent electron emission process accompanying α-decay. If, however, the electron shell in the final state is an excited state, caused either by IC or by inner-shell SO, we calculate the full atomic RX, which will be described in detail in section 3.1.

3. Implementation into the simulation software

To study the event topologies of electrons from the α-decay of ^{219,220}Rn atoms, and to estimate background rates and characteristics due to their subsequent trapping (for details, see [9, 10]), a detailed code for particle trajectory calculations in the complex electromagnetic field configuration of the KATRIN spectrometer is required. This challenging task is met by the KATRIN simulation package KASSIOPEIA [32], which was validated by a variety of different measurements [10, 12, 13, 33]. A Monte Carlo event generator was developed to model electron emission following ^{219,220}Rn α-decay and is described in section 3.1. Section 3.2 then gives a short overview of the output of this generator.

3.1. The radon event generator

The detailed physical model for signal events and background processes is implemented into the KASSIOPEIA package via Monte Carlo (MC)-based event generators. For the investigations of this paper, a radon background generator was developed to describe the processes accompanying the initial radon α-decay, such as IC, SO, RX and SR which are described in the previous section 2.

Figure 3 shows a flowchart of the radon event generator.

The simulation can be configured by the user to study the impact of different processes on the background. The following choices are available (options in parentheses):

- activate/deactivate individual physical processes (SO, IC, SR, RX),
- enforce physical processes (SO, IC),
- select radon isotope (219, 220).

During initialization, all data files required for the computation of the various physical processes for a specific isotope are read in. Enforcing SO and IC processes can be useful because they are rather rare (up to few %). If this option is enabled, the emission probabilities of the individual shells are scaled up until their sum totals 100%. In doing so, it is assured that the SO and/or IC processes are executed within every generated event.

The first physical process to be carried out (if activated by the user) is the SO process, as it is directly caused by the passage of the α-particle through the atomic shell. At first a random number is generated by the ROOT TRandom3 routine, which is based on the Mersenne Twistor algorithm [34]. The SO subroutine then uses the generated random number to initiate an SO process with the corresponding probabilities for the individual (sub-)shells. Consequently, this can in some rare cases result in the emission of multiple SO electrons [20]. For the determination of the SO electron energy the acceptance–rejection method [35] is applied to (2).

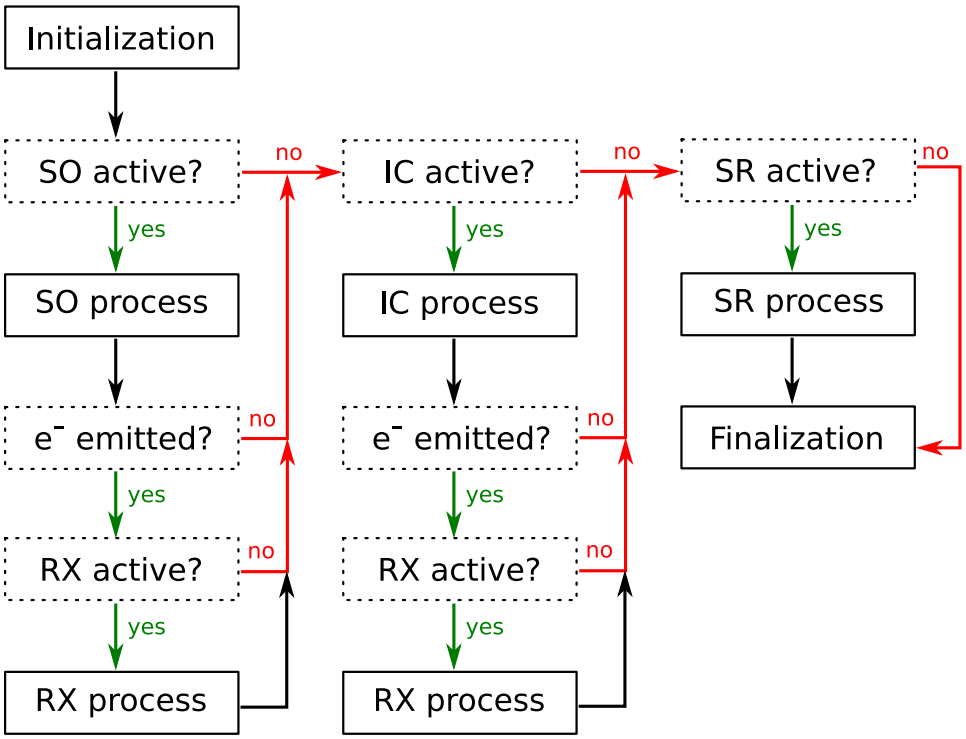

Figure 3. Event generator flowchart: after initialization of the generator, the different physical processes (SO, IC, RX and SR), represented as solid boxes, are processed according to the model, which is described in more detail in the main text. The user has the possibility to configure the generator, e.g. turn on or off certain processes to study specific aspects. Corresponding decision points are given in dashed boxes.

If any SO electrons were generated, the RX process will be executed (if activated by the user). In our routine we employ the Monte Carlo technique [36] to simulate the highly complex pathways of an initial single vacancy, where a large number of intermediate electron shell configurations is being involved. In a first step, we use the fluorescence yield ω_{i} and the Auger yield α_i of the shell i which is under investigation to determine the transition type. For K- and L-shell vacancies the data of [37], and for M- and N-shell vacancies those of [38, 39] is used. If a radiative transition is diced, the vacancy is simply transferred to a higher shell, where the new vacancy is determined from the available final states according to their relative probabilities. Non-radiative transitions up to and including the M-shell result in two vacancies, while several vacancies can be created by N-shell vacancy de-excitation due to super-Coster–Kronig transitions, i.e. all transitions happen within the N-shell. The described process is repeated until all vacancies reach the outer O- or P-shells or until no further de-excitations are energetically possible. As we do not take into account small modifications of the energies of electron shells due to the actual RX process, the de-excitations result in discrete energy lines.

After the RX process was completed, or if, initially, the SO process was deactivated, the IC process is performed (if activated by the user). This specific ordering is justified by the fact that shell RX processes are completed on a much faster time scale (10^{-15} s) [40] than IC processes (10^{-12} s) [41]. As in the SO subroutine, a random number is used to initiate an IC process

with the correct probability. Because the excited nucleus can decay into an intermediate energy state instead of the ground state, this has to be taken into account by allowing consecutive IC processes (so called double conversion [22]). The interrelated energy levels are marked as such in the input file, which allows for reliable bookkeeping of the involved states. The IC electron energy depends solely on the decaying nuclear state and the binding energy of the emitted electron, resulting in discrete IC lines.

The final process to be carried out is the SR process. At first, the SR subroutine checks if any SO or IC processes occurred previously. If this is the case, the SR process is skipped because the Po daughter has already relaxed via the above mentioned processes. Otherwise, an unperturbed shell is assumed, which results in the excitation of two electrons, statistically sharing the SR energy of $\Delta\overline{E_R} = 250\,\text{eV}$ (shell binding energy to be deducted). These electrons are actually only emitted from the atom if their energy exceeds the outer shell binding energy of about 1 eV (first ionization) or 9 eV (second ionization).

In the final step of the event generation, all electrons generated by a single α-decay are passed to the particle tracking part of the KASSIOPEIA simulation software.

3.2. Generator output

Figure 4 shows the energy spectra as obtained with our event generator. The discrete IC and RX lines, as well as the higher-order potential dependence of the SO spectrum can be clearly identified. The flat energy spectrum dominating the low-energy part is originating from our model of SR electrons in case of negligible atomic shell perturbation ($6p^6 \rightarrow 6p^4$), as the two electrons statistically share an energy of 230–250 eV. Due to their identical nuclear charge, the inner-shell SO and SR contributions of the two polonium isotopes are assumed to be identical. The SO probability is negligible for the inner K-shell. Therefore, the low-energy part of the RX spectrum results mainly from L-shell (or higher) SO, and hence reaches up to about 17 keV (L-shell binding energy). As stated above, the IC process is of importance only in the decay $^{219}\text{Rn} \rightarrow {}^{215}\text{Po}^*$. In this case, there is a high probability for vacancies in the inner K-shell, leading to the high-energy part (up to about 90 keV) of the RX spectrum.

The total probability for electron emission by a specific process can be obtained by integration over the whole energy spectrum. The corresponding results are summarized in table 3.

3.3. Initial test of the model

Due to the complex nature of the response of the atomic shells during and after the emission of an α-particle, it is of vital importance to compare the present model with independent measurements. Generic parameters for comparison are:

(i) the final charge state of the daughter atom, because it is highly sensitive to a correct description of processes such as atomic RX, and

(ii) the electron energy spectrum in the multi-keV range, which can be estimated from the number of secondary electrons produced in the electrostatic spectrometer [10].

Figure 5 shows the polonium charge state following ^{219}Rn and ^{220}Rn decays as obtained with the generator of this work, in comparison to the independent measurement reported in [26]. The Po charge state is obtained from the electron multiplicity by subtracting a charge of two

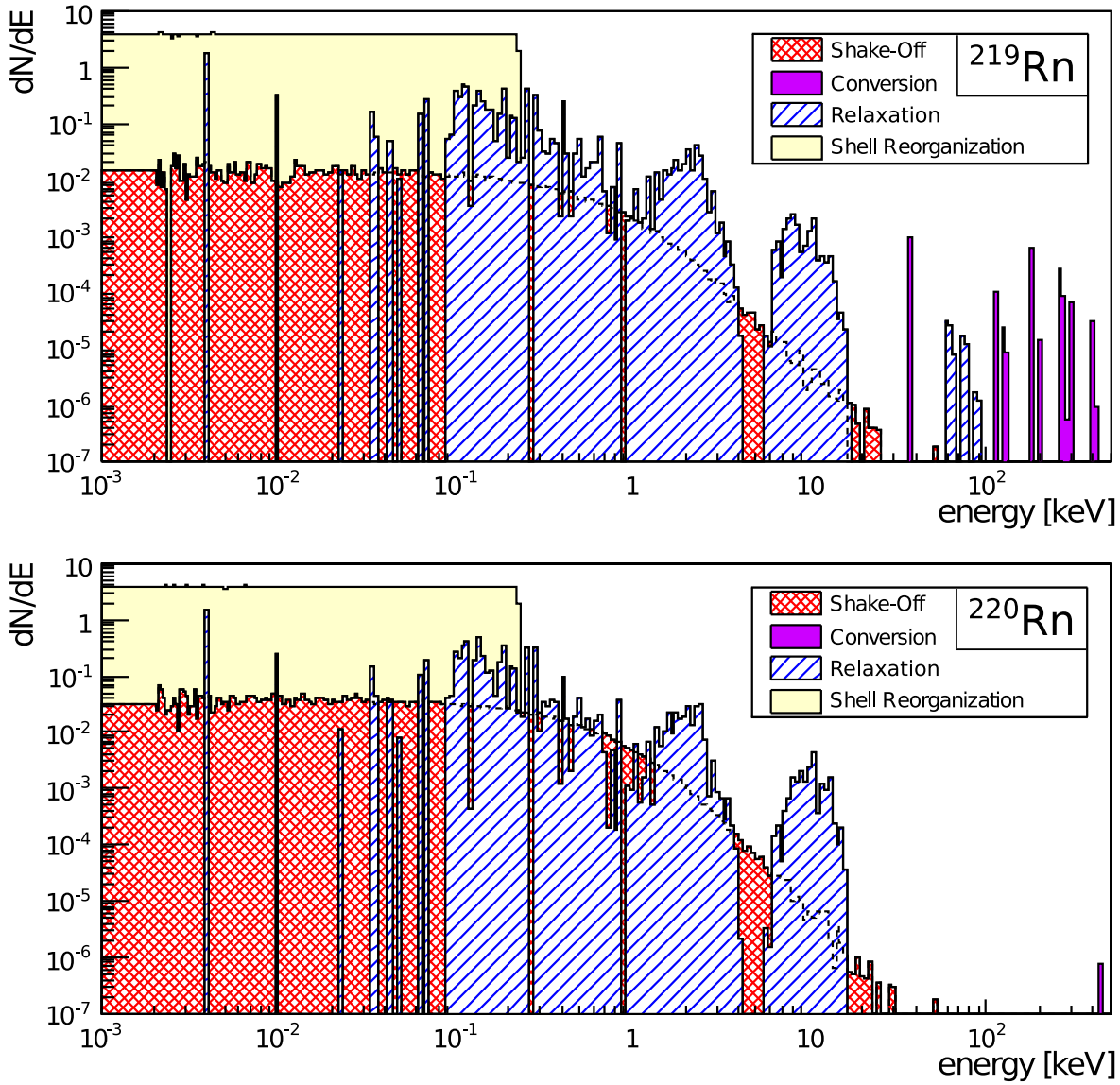

Figure 4. Event generator: energy spectra of IC, inner-shell SO, RX and SR electrons for the case of ^{219}Rn $\rightarrow^{215}$ Po (top) and ^{220}Rn $\rightarrow^{216}$ Po (bottom) α-decay. SR electrons, which originate from unperturbed atomic shell RX, are distinguished from K-, L- and M-shell SO electrons. The electron energy axis is subdivided into 250 intervals between 1 and 500 keV with logarithmically increasing bin size.

to compensate for the emitted α-particle. There is good agreement between measured and simulated frequencies of occurrence of different ^{216}Po charge states, which underlines the basic validity of our model. We attribute the deviations occurring at charge states $\geqslant 6$ to the complex nature of atomic RX paths, which can only be approximated for the outer shell electrons in case of a large initial perturbation of the atomic shell system.

As can be seen in figure 5, the majority of events consists of two low energetic SR electrons. When comparing the experimental data of [26] with our Monte Carlo generator we note that the

Table 3. Electron emission probabilities P per decay, depending on the emission process, based on the ^{219}Rn and ^{220}Rn event generators of this work. $P > 1$ implies that more than one electron can be emitted per decay.

Process	P (^{219}Rn)	P (^{220}Rn)
Inner-shell SO	2.08×10^{-2}	2.15×10^{-2}
IC	3.31×10^{-2}	5.0×10^{-5}
RX	2.29×10^{-1}	6.81×10^{-2}
SR	1.89	1.96

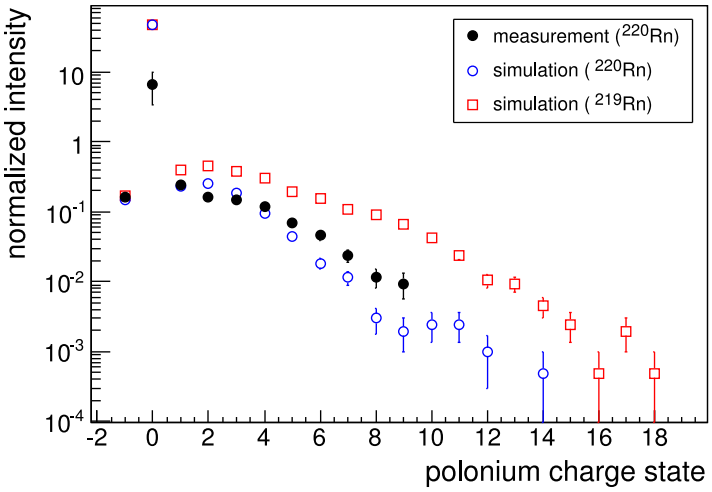

Figure 5. Charge states of ^{216}Po (daughter of ^{220}Rn) and ^{215}Po (daughter of ^{219}Rn), as obtained with our generator. The simulation is compared to an independent measurement of the ^{216}Po charge state [26], which was also performed for gaseous radon in vacuum. In the original publication, the mean intensity values for each charge state were normalized to the value of charge state +1. For better comparison in this publication, we chose to normalize both the measurement of [26] and the values obtained with the ^{220}Rn generator of this work to the overall rate of non-zero charge states as the experimental precision for the detection of neutral daughter atoms was rather limited in [26]. For the ^{219}Rn results, the same normalization constant was used to emphasize the difference between the two isotopes.

detection of neutral daughter states, as outlined in [26], was rather challenging. We thus ascribe the discrepancy to experimental difficulties in assessing the efficiency in detecting neutral atoms after α-decay.

The significant difference between the two simulated isotopes in electron multiplicities, and correspondingly in the charge distribution of the daughter ion, is due to IC processes in the case of $^{219}\text{Rn} \rightarrow ^{215}\text{Po}^*$. As they are emitted from inner shells, highly charged final states result from complex RX cascades.

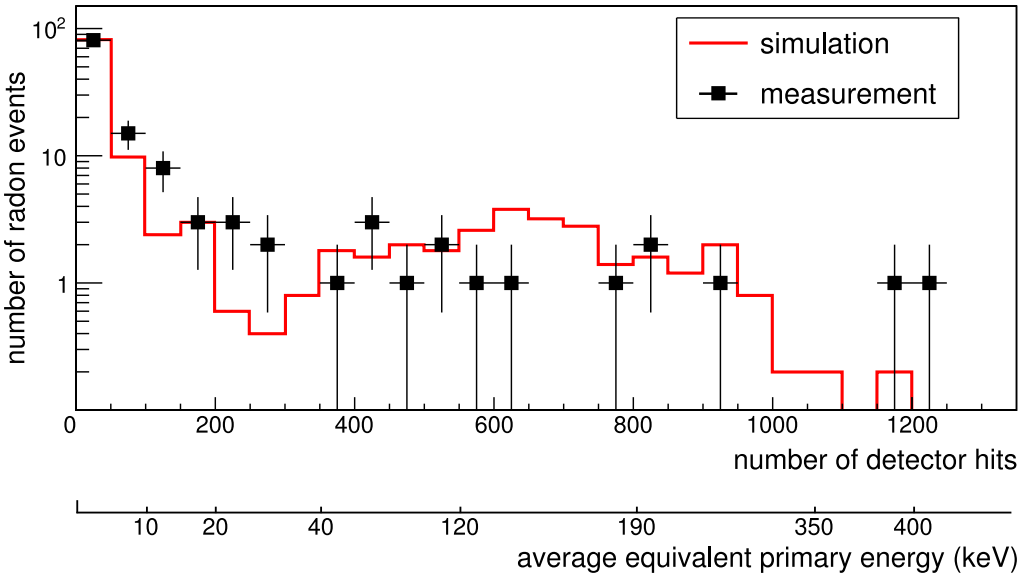

Figure 6. Comparison of measured and simulated numbers of detector hits produced by individual radon α-decay events within the KATRIN pre-spectrometer. An equivalent energy scale can be reconstructed when using average energy losses due to scattering and synchrotron radiation [10]. The nonlinearity of the energy scale results from the decreasing scattering cross section for higher energies in combination with linearly increasing synchrotron losses.

The second important parameter which is of key importance to validate our model is the energy spectrum of the emitted electrons in the multi-keV range. In an electrostatic spectrometer of the MAC-E filter type, this parameter cannot be measured directly, as high-energy electrons are trapped over long periods of time [3, 9–13]. However, an indirect method to assess the energy of magnetically stored multi-keV electrons is to make use of their subsequent cooling via ionization of residual gas and to count the number of produced secondary electrons in a detector. The electromagnetic configuration of the pre-spectrometer MAC-E filter causes all electrons with transversal kinetic energies $E_\perp > 60\,\mathrm{eV}$ to be stored [10]. As the majority of the secondary electrons is found to have $E_{\mathrm{kin}} = E_\perp + E_{||} < 100\,\mathrm{eV}$ [13], where $E_{||}$ is the longitudinal energy component, their storage probability is rather low. Measurements and corresponding simulations showed that a single radon α-decay can lead to a large number of detector hits N_{det} (up to 1500 hits corresponding to a single event were observed at the KATRIN pre-spectrometer). There is a good correlation between primary electron energy (shown in figure 4) and N_{det}, which is, however, not strictly linear due to competing energy losses by synchrotron radiation and due to non-adiabatic effects at higher energies. In figure 6 we display the number of detector hits following single radon α-decays in the KATRIN pre-spectrometer in an experimental configuration where ionizing collisions with residual gas (Ar at $p = 2 \times 10^{-9}\,\mathrm{mbar}$) were maximized at the expense of synchrotron losses. The measured spectrum is compared to corresponding Monte-Carlo simulations with the radon generator of this work. In a separate publication [10] we have determined the ^{219}Rn and ^{220}Rn activities in the spectrometer, which were used as a basis for the simulations presented in figure 6. There is

good agreement between experimental data and MC simulation, taking into account the limited number of radon α-decays (127 events) accumulated over a measuring period of about 500 h. The simulation reproduces the main features of the measured distribution: a large number of Rn-events with rather few detector counts, caused by the low-energy plateau of the SO events, and a steep decrease (tail of the SO spectrum) toward a flat plateau of very few events featuring a large number of detector hits (caused by conversion electrons).

4. Conclusions

In the course of this work we have developed for the first time a comprehensive and detailed model of electron emission processes following the α-decays of the two radon isotopes ^{219}Rn and ^{220}Rn. These investigations were motivated by our earlier observations, reported in [3], of periods with significantly enhanced background rates at the KATRIN pre-spectrometer measurements.

The background model incorporates various processes such as IC, SO and RX of the atomic shells during or after the α-emission. The resulting electron energies cover a wide range between a few eV up to several hundred keV, and involve highly charged polonium daughter ions. Our model successfully reproduces experimentally observed polonium charge states as well as electron energies in the multi-keV range, as shown in this work. A combination of the model of this work with precise electron trajectory calculations provides the necessary thorough understanding in order to reduce the background level below the required limit. Therefore, further experimental validation of our complete physics model was performed in a separate work [10], where the background behavior observed within test measurements at the KATRIN pre-spectrometer could be well described. It is only by developing and by validating detailed models of background processes that the KATRIN experiment can realize its full physics potential in measuring the absolute mass scale of neutrinos.

Acknowledgments

This work was supported in parts by the Bundesministerium für Bildung und Forschung (BMBF) with project number 05A08VK2 and the Deutsche Forschungsgemeinschaft (DFG) via Transregio 27 'Neutrinos and beyond'. We thank the Karlsruhe House of Young Scientists (KHYS) of KIT for their support (SG, SM, NW). We acknowledge support by DFG and Open Access Publishing Fund of Karlsruhe Institute of Technology.

References

[1] Angrik J *et al* 2004 KATRIN design report *FZKA Report* 7090
[2] Drexlin G *et al* 2013 *Adv. High Energy Phys.* **2013** 293986
[3] Fränkle F M *et al* 2011 *Astropart. Phys.* **35** 128–34
[4] Beamson G, Porter H Q and Turner D W 1980 *J. Phys. E: Sci. Instrum.* **13** 64–6
[5] Lobashev V M and Spivak P E 1985 *Nucl. Instrum. Methods* A **240** 305–10
[6] Picard A *et al* 1992 *Nucl. Instrum. Methods* B **63** 345–58
[7] Wolf J 2009 *J. Vac. Soc. Japan* **52** 278–84
[8] Higaki H, Ito K, Kira K and Okamoto H 2008 *AIP Conf. Proc.* **1037** 106–14
[9] Mertens S *et al* 2013 *Astropart. Phys.* **41** 52–62

[10] Wandkowsky N, Drexlin G, Fränkle F M, Glück F, Groh S and Mertens S 2013 *J. Phys. G: Nucl. Part. Phys.* **40** 085102
[11] Fränkle F M 2010 Background investigations of the KATRIN pre-spectrometer *PhD Thesis* Karlsruhe Institute of Technology
[12] Mertens S 2012 Study of background processes in the electrostatic spectrometers of the KATRIN Experiment *PhD Thesis* Karlsruhe Institute of Technology
[13] Wandkowsky N 2013 Study of background and transmission properties of the KATRIN spectrometers *PhD Thesis* Karlsruhe Institute of Technology
[14] Mertens S *et al* 2012 *J. Instrum.* **7** P08025
[15] Sonzogni A 2012 *National Nuclear Data Center, Brookhaven National Laboratory* (www.nndc.bnl.gov/chart)
[16] Siegbahn K 1968 *Alpha-, Beta- and Gamma-Ray Spectroscopy* vol 2 (Amsterdam: North-Holland) p 894
[17] Theisen Ch, Lopez-Martens A and Bonnelle Ch 2008 *Nucl. Instrum. Methods* A **589** 230–42
[18] Browne E 2001 *Nucl. Data Sheets* **93** 763–1061
[19] Wu S C 2007 *Nucl. Data Sheets* **108** 1057–92
[20] Freedman M S 1975 Ionization by nuclear transitions *Summer Course in Atomic Physics* (Carry-le-Rouet, France: Argonne National Laboratory)
[21] Hansen J S 1974 *Phys. Rev.* A **9** 40–3
[22] Freedman M S 1974 *Annu. Rev. Nucl. Sci.* **24** 209–48
[23] Bang J and Hansteen J M 1959 *K. Dan. Vidensk. Selsk. Mat.-Fys. Medd.* **31** 1–43
[24] Rapaport M S, Asaro F and Perlman I 1975 *Phys. Rev.* C **11** 1740–5
[25] Rapaport M S, Asaro F and Perlman I 1975 *Phys. Rev.* C **11** 1746–54
[26] Szucs S and Delfosse J M 1965 *Phys. Rev. Lett.* **15** 163–5
[27] Migdal A 1970 *J. Phys. USSR* **4** 449
[28] Burhop E H S 1952 *The Auger Effect and Other Radiationless Transitions* (Cambridge: Cambridge University Press)
[29] Larkins F P 1977 *At. Data Nucl. Data Tables* **20** 311–87
[30] Pomplun E 2000 *Acta Oncol.* **39** 673–9
[31] Lu C C *et al* 1971 *At. Data* **3** 1–131
[32] Furse D *et al* 2013 KASSIOPEIA—the simulation package for the KATRIN experiment (submitted)
[33] Prall M *et al* 2012 *New J. Phys.* **14** 073054
[34] Mathsumoto M and Nishimura T 1998 *ACM Trans. Model. Comput. Simul.* **8** 3–30
[35] Robert C and Casella G 2004 *Monte Carlo Statistical Methods* (*Springer Texts in Statistics* vol 47) (Berlin: Springer)
[36] Pomplun E, Booz J and Charlton D E 1987 *Radiat. Res.* **111** 533–52
[37] Chen M H, Crasemann B and Mark H 1979 *At. Data Nucl. Data Tables* **24** 13–37
[38] McGuire E J 1972 *Phys. Rev.* A **5** 1043–7
[39] McGuire E J 1974 *Phys. Rev.* A **9** 1840–51
[40] Drescher M *et al* 2002 *Nature* **4198** 803–7
[41] McCamant D W, Kukura P and Mathies R A 2003 *J. Phys. Chem.* A **107** 8208–14